

*Original Research*

# A 3S-based Regional Terrestrial Carbon Cycle Model in Luanhe Basin, China

Tianling Qin<sup>1</sup>, Fang Liu<sup>1,2\*</sup>, Shanshan Liu<sup>1</sup>, Jian Li<sup>1,3</sup>, Jie Lu<sup>1</sup>, Xiuyan Zhang<sup>1,4</sup>

<sup>1</sup>State Key Laboratory of Simulation and Regulation of Water Cycle in River Basin, China Institute of Water Resources and Hydropower Research, No. 1 Fuxing Road, Haidian District, Beijing 100038, China

<sup>2</sup>College of Environmental Science and Engineering, Donghua University, No. 2999 Renminbei Road, Songjiang District, Shanghai 201620, China

<sup>3</sup>School of Environment, Liaoning University, No. 66 Chongshan Middle Road, Huanggu District, Shenyang 110036, China

<sup>4</sup>College of Resource Environment and Tourism, Capital Normal University, No.105 West Third Ring Road North, Haidian District, Beijing 100048 China

*Received: 9 January 2023*

*Accepted: 21 April 2023*

## Abstract

For a comprehensive response to climate change and low carbon development mode, the 3S-based regional terrestrial carbon cycle model in Luanhe basin is constructed in accordance with component-based development strategy to identify carbon cycle evolution of terrestrial ecosystem under the background of local changes, combining measured weather data, prototype observation data of soil and plants as well as remote-sensing information in different spatial and temporal scales. The model has the ability of describing canopy fluxes, net primary productivity, biomass allocation and turnover, mortality, decomposition of soil organic matter and other dynamic processes. The carbon cycle evolution in Luanhe Basin from 1995 to 2010 is simulated and analyzed. The results are shown as follows: 1) in the temporal scale, inter-annual change of leaf area index with a slight growth trend is larger than that of net primary productivity (*NPP*), ground and underground biomass and soil carbon content; 2) There are obvious regional differences in spatial view, spatial distribution of results are consistent with those of watershed plant and soil, displaying the characteristics that the above major variables of mountainous regions in middle-upper reaches are greater than those of grassland meadows in the upstream and plains in the downstream.

**Keywords:** carbon cycle model, climate change, Luanhe Basin, terrestrial ecosystems

## Introduction

Since the Industrial Revolution, emissions of carbon dioxide, carbon monoxide and other greenhouse gases in the environment have exploded due to the massive burning of fossil fuels and land use changes [1-4]. This is a key factor contributing to global warming. According to statistics, compared with the beginning of the Industrial Revolution (1750), the concentration of carbon monoxide in the atmosphere will increase by 49.7% in 2021 [5]. IPCC predicts that by the end of this century, the global average temperature will rise by 0.3-4.8°C, the sea level will rise by 0.26-0.82 m, and the volume of glaciers will decrease by 15%-85% [6]. These changes may cause frequent extreme weather, reduce ecosystem services and biodiversity, and directly affect human life and the health and safety of terrestrial ecosystems [7-9]. Therefore, reducing greenhouse gas emissions and increasing the carbon uptake capacity of vegetation is the key to sustainable development of terrestrial ecosystems [10-11].

Terrestrial ecosystems are the world's largest carbon sink with the most complex feedback mechanisms, offsetting more than 30% of anthropogenic carbon emissions each year [12-13]. In order to capture and understand the factors affecting the change of the terrestrial ecosphere, more and more studies focus on the terrestrial carbon cycle [14-15]. As the major influential factor of global climate changes, carbon cycle has turned to be one of basic material cycling for keeping ecosystem stable and achieving the sustainable development between economic-society and eco-environment [16-17]. The terrestrial carbon cycle is an extremely complex process, involving physical, chemical and biological processes, generally directly related to the atmosphere, vegetation, litter, soil, etc., and also affected by environmental parameters such as temperature, precipitation, radiation, and land use [18-20].

In the process of comprehensive response to global climate changes and low carbon mode, carbon cycle simulation technology is so significant to explore the characteristics and trends of temporal and spatial changes in the carbon cycle process [21-22]. At present, the main methods commonly used to estimate the terrestrial carbon cycle include field experiments, remote sensing estimation and model simulation [23-24]. Field experiments can quantify actual vegetation in real time including long-term observation field, natural gradient studies and small-scale control experiment [25]. Remote sensing estimation is usually combined with geographic information technology to obtain various vegetation state parameters, and then quantify large-scale vegetation carbon storage [26-27]. The carbon cycle modeling could identify continuous dynamic evolution characteristics of carbon cycle in a large spatial-temporal scale, and obtain the continuous historical sequence of vegetation carbon pools (including leaves, stems and roots), soil carbon storage/flux

and shift flux to overcome the technical limitations of spatial and temporal scales [28-29]. For example, Liu et al. used the Boreal Ecosystem Productivity Simulator (BEPS) model to study the changes in China's ecosystem NPP from 2000 to 2010 [30]. Lindeskog et al. estimated the carbon balance of European forests using the Lund-Potsdam-Jena General Ecosystem Simulator (LPJ-GUESS) model, which showed a 32% increase in simulated total carbon from 1991 to 2015 [31]. Tong et al. used satellite data and Lund-Potsdam-Jena (LPJ) models to reveal that the vegetation ABC in China's karst areas increased by 9% after 2001 [32]. "Two pools" were applied to global carbon cycles for simulating carbon balance of ecosystem by Since Craig in 1950s [33]. Multi-dimension development has been achieved based on photosynthesis and respiration mechanism. From the view of ecosystem type, many kinds of carbon cycle models applicable to the terrestrial (forest, grassland, farmland, city and etc.) and water (marine, wetland and etc.) have been researched aiming at special characteristics of different ecosystems. Among them, the researches on forest, grassland, marine and wetland are more mature while in a small number city and river. On the aspect of large scale, according to the development of coupled carbon cycle, AGCM and water cycle model, a considerable progress has been made in regional and global carbon cycle mode (Fig. 1) [34-50].

China's carbon balance forest coverage rate in terrestrial ecosystems is 22.96%, which is an important part of the global carbon cycle [51]. As the world's second economy, China has become the world's largest emitter of greenhouse gases, accounting for more than 27% of global greenhouse gas emissions [52]. China has committed to reaching the peak of carbon emissions in 2030 and achieving carbon neutrality before 2060 [53]. Therefore, accurate quantification of China's terrestrial carbon cycle is crucial for global climate change. Nevertheless, terrestrial carbon cycle models for plant distribution in China are in a small number recently. As a result, in order to slow down disadvantage effects of climate changes on eco-environment, it is necessary to build regional terrestrial carbon cycle model on account of plant distribution in China from the view of current research to understand regional ecological evolution.

Located in an important position of regional water resource allocation as a secondary water district of Haihe Basin, Luanhe Basin is one of significant water sources for strategic economic circle around Bohai Sea, including Tianjin, Tangshan, Caofeidian and other cities. Recently, "involved water" and "involved land" troubles are brought by diverted ecological water and land, such as water resource efficiency, water pollution aggravation and water ecological degeneration, further inducing a reduction of carbon sink [54]. To solve the above practical problems and identify regional carbon cycle evolution and change characteristics of key components, on a basis of carbon balance mechanism, plant and soil were taken as research objects in this study to construct

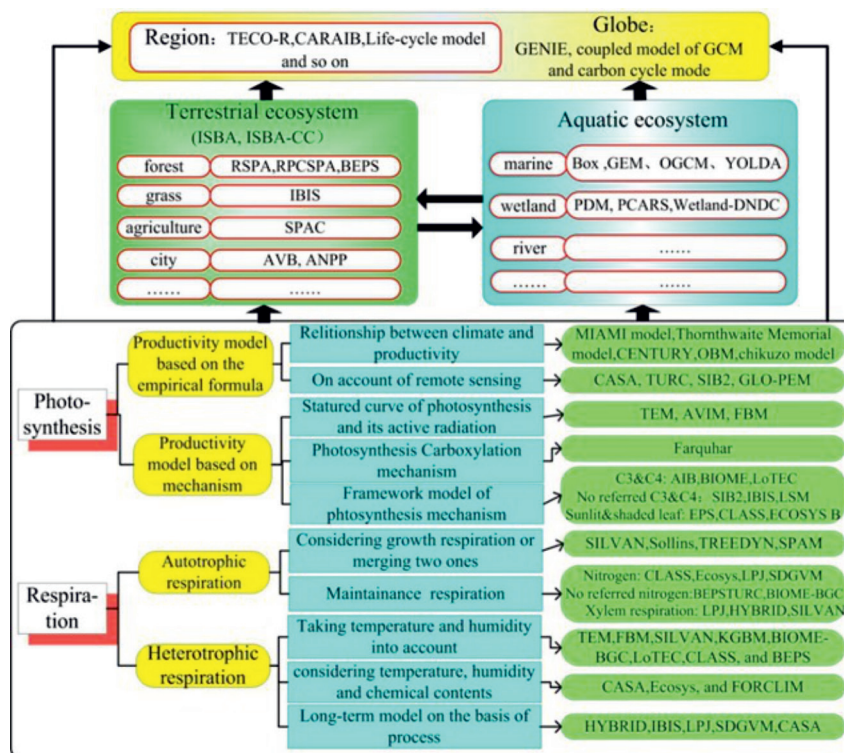


Fig. 1. Research system of carbon cycle model based on biochemical process such as photosynthesis and respiration.

the 3S-based regional terrestrial carbon cycle model in Luanhe Basin. Then, a vital technological support will be provided for mitigating eco-environmental problems, promoting efficient management of ecological system and building low-carbon environment-friendly society.

## Materials and Methods

### Study Site

The Luanhe Basin (115°34'-119°50', 39°02'-42°43') is located in the northeast of the North China Plain. The main stream has a total length of 888 km and a drainage area of 545000 km<sup>2</sup>, of which the mountainous area accounts for 74.11% and the plain area accounts for 25.89%. The drainage system of Luanhe Basin consists of Luanhe and coastal rivers in East Hebei

### Regional Terrestrial Carbon Cycle Model

Based on the physical, chemical and biological theories of Community Land Model (CLM) [56], Dynamic Global Vegetation Model (DGVM) [57] and the Community Land Model's Dynamic Global Vegetation Model (CLM-DGVM) [58], a serial process of physics-chemistry-biology is considered as well as the interaction among individuals in the 3S-based regional terrestrial carbon cycle model of Luanhe Basin. Then, dynamic phenology of different plant types can be simulated in the study area.

### Construction Strategy

Considering regional characteristics of plant types, canopy fluxes, net primary productivity, biomass allocation and turnover, mortality, decomposition of soil organic matters and other processes are described in the regional terrestrial carbon cycle model based on dynamic physical mechanism of ecosystem.

According to the physics-chemistry-biology process of carbon in vegetation and soil, component-based development strategy is developed in this model with a number of modules. Canopy fluxes module describes the change of energy and water fluxes, whose brief theory is energy balance. In particular, net radiation among the atmosphere, soil and ecosystem involves three aspects, including surface heat flux, latent heat flux and sensible heat flux. Interaction between the latter two parts could directly influence the temperature and water fluxes of soil and canopy, and change evapotranspiration. Meanwhile, variation of wind speed and roughness length will affect the resistance of canopy boundary layer. Photosynthetic active radiation, as one storage form of ecosystem net radiation, is the major driver of producing organic matter for other biophysical processes. All factors above in the canopy fluxes will determine the photosynthetic rate and biomass production. With the allometric growth of plants, biomass increment is allocated in a certain percentage to the leaf, sapwood, heartwood and root respectively. The process could change some typical plant index, such as leaf area index, foliage projective cover, height, crown area of individual,

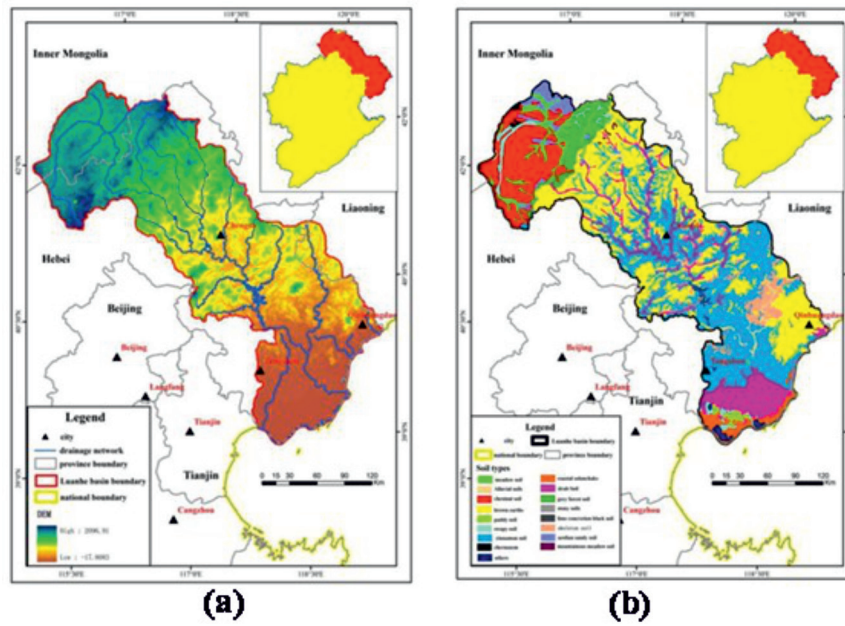


Fig. 2. Drainage system and soil type of Luanhe Basin: a) drainage system; b) soil type.

which is constantly updated and become initial values for the next time step. According to the tissue longevity, the turnover module could represent that the amount of living biomass enters the above and below ground litter and the amount of sapwood turns to heartwood. Due to the stress of surface temperature and natural rhythm, some individuals are removed and converted to litters. Then, litters above and below the ground are decomposed and turn to be soil carbon in response to

microbial respiration. Details of calling sequence and logic relationship among modules are shown in Fig. 3.

Model Structure

1) Horizontal structure

The study area is divided into square grids, subdivided by the Mosaic Law based on plant function types. It consists of waters, bare-land, plant area and

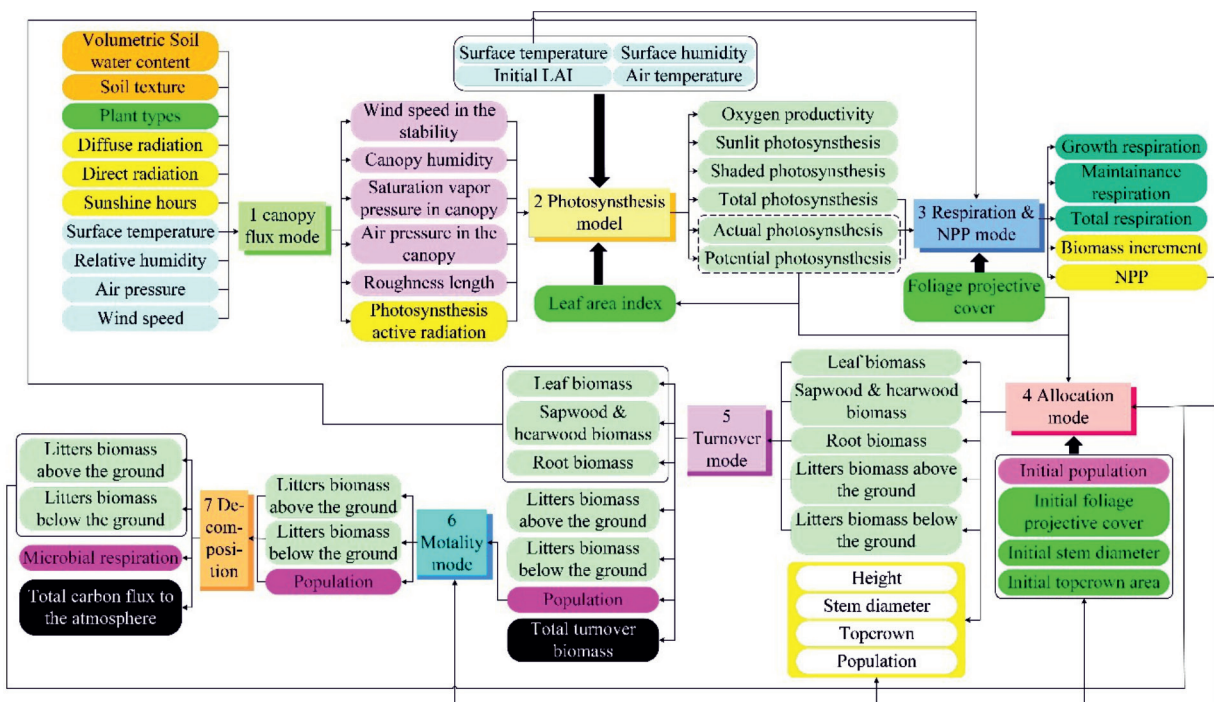


Fig. 3. Calling sequence and logic relationship of the model.

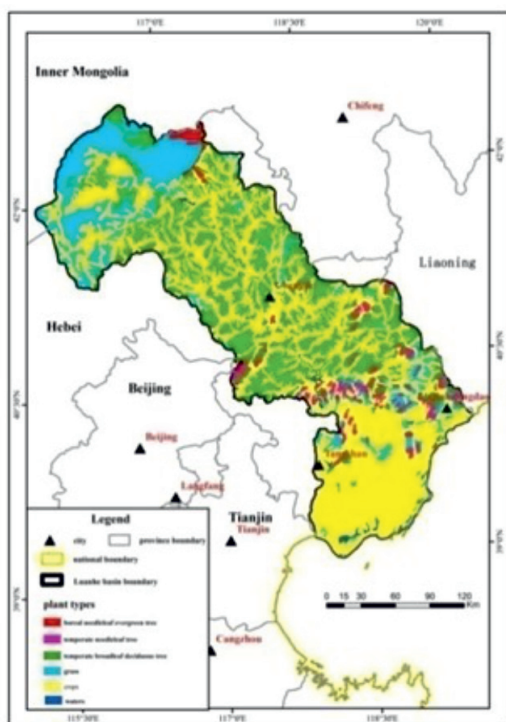


Fig. 4. Plant subgroup distribution in Luanhe Basin.

permeable waters. The plant area is reconstructed in Luanhe Basin, comprised of temperate needle-leaf evergreen trees, temperate broadleaf deciduous trees, boreal needle-leaf evergreen trees, boreal deciduous trees, grasses, crops and waters (Fig. 4).

## 2) Vertical structure

The general vertical structure of terrestrial ecological system is divided by atmospheric layer, plant area (including canopy, sapwood, heartwood and root), litter and soil layer. Carbon and energy exchanges exist between atmosphere and plant area. Carbon dioxide in the atmosphere could be captured in the canopy and transformed into organic matter which is allocated to other tissues. Withered leaves and sapwood will become litters on surface, while undecomposed parts and corrupted roots will reach soil layer. In surface litter and soil layer, carbon pools are divided into two types, i.e., the faster decomposing pool and the slower one (Fig. 5). CO<sub>2</sub> produced by the respiration of plants as well as soil heterotrophic respiration will be back to the atmosphere.

### Input Data and Its Processing

Major input data of RTCCM-3S could be classified into three types, i.e., meteorological, plant and soil data (Table 1). With the “Analysis Tools>Create Thiessen Polygons” in the Arc-map, Thiessen polygons will be obtained from meteorological and radioactive monitoring sites. Subsequently, spatial distribution of data could be available. Plant data are reclassified to produce ASCII file by Visual Basic (VB), and leaf area index (LAI) and foliage projective coverage are extracted with ENVI4.7. For soil data, it is necessary to combine field prototype soil data with plant distribution to produce soil data based on plant types.

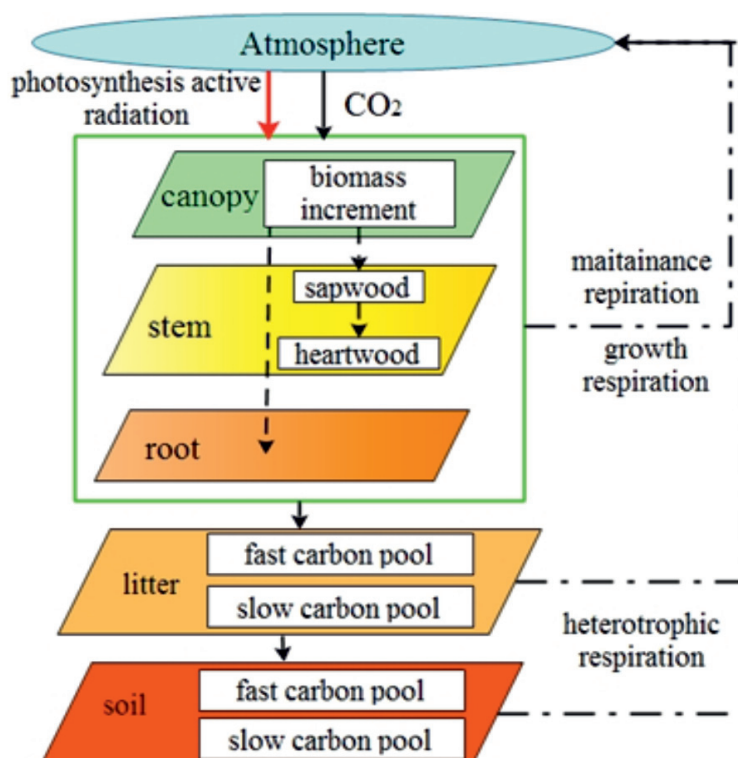


Fig. 5. Vertical structure of the regional terrestrial carbon cycle model.

Table 1. Input data and source of the model.

Type	Major data	Source	Description
Meteorological data	Surface temperature	China meteorological data sharing network	Daily observations of meteorological stations
	Relative humidity		
	Wind velocity		
	Atmospheric pressure		
	Sunshine hours		
	Diffuse radiation		Daily observations of radiation stations
	Direct radiation on the vertical		
Plant data	Initial leaf area index	Remote sense images from LANDSAT and MODIS	Extracted by ENVI 4.7
	Foliage projective coverage		
	Plant types	China vegetation distribution map	Vegetation subgroups
Soil data	Soil texture	Soil survey data, soil database and field prototype	Combine current data with field prototype data
	Volumetric water content		

### Simulation of Key Processes

#### 1) Canopy fluxes

Eight modules are employed in the process to simulate energy and water fluxes change between atmosphere and soil, especially for the canopy (Table 2). Then, the evolution of water vapor, sensible heat and latent heat is shown in vegetation covered area on the basis of canopy energy balance mechanism. Taking the canopy flux as the driving and basic process, photosynthesis, respiration, net primary productivity, biomass allocation and turnover, mortality, decomposition and other process are improved, and details are as followed.

#### 2) Photosynthesis

Photosynthesis rate is comprehensively influenced by factors, including the storage of Ribulose Diphosphatecarboxylase (RuBP), rate of energy transferring and the export limited rate of carboxylation.

Carboxylation rate of RuBP ( $W_c$ ) is described as the storage of RuBP, which could represent actual and potential ( $V_{max}$ ,  $V_{max\ pot}$ ) as the comprehensive function about temperature and water content. Then, actual and potential photosynthesis ( $W_{ca}$ ,  $W_{cp}$ ) could be obtained. The light-limited rate ( $W_j$ ) becomes the comprehensive function of photosynthesis active radiation ( $\phi$ ) and the capacity of light transferred. With the sunlit and shaded leaf area index ( $L_{sun}$ ,  $L_{sha}$ ),  $W_j$  of them will be derived respectively. The export rate of productivity ( $W_e$ ) could be characterized by the empirical function of maximum carboxylation rate. Its derivation of specific parameters is the same to CLM-DGVM.

In the model, minimum value among  $W_c$ ,  $W_j$  and  $W_e$  is selected as photosynthesis rates [59-60]. On the basis of current theory and mechanism above, the photosynthesis of sunlit and shaded leaves ( $A_{asun}$ ,  $A_{asha}$ ) is added into this process to derive total photosynthesis rate with their leaf area indexes.

$$A = A_{asun} \times L_{sun} + A_{asha} \times L_{sha} \quad (1)$$

According to the formula of photosynthesis process, the mole number of  $O_2$  production is equal to that of  $CO_2$  consumption. Then, oxygen productivity will be derived.

#### 3) Autotrophic respiration

The energy from autotrophic respiration is supplied to the growth of leaf, sapwood, heartwood and root. The respiration ( $R_a$ ) can be divided into two parts: growth and maintenance respiration ( $R_g$ ,  $R_m$ ).

$$R_a = R_g + R_m \quad (2)$$

$$R_g = 0.25(A - R_m) \quad (3)$$

$$R_m = \sum R_{tissue} \quad (4)$$

$$R_{tissue} = r \cdot k \frac{C_{tissue}}{cn_{tissue}} \phi \cdot g(T) \cdot \frac{2 \times 10^6 P}{28.5 \cdot FPC} \quad (5)$$

where  $R_a$  ( $\mu mol_{CO_2}/m^2s$ ) is the growth respiration rate of vegetation;  $R_m$  ( $\mu mol_{CO_2}/m^2s$ ) is the sum of maintenance respiration rate of tissue ( $R_{tissue}$ ), including the leaf, sapwood and root;  $r$  ( $gC/gN$ ) is the subordinate index of respiration (Table 3);  $k$  represents  $6.34 \times 10^{-7} s^{-1}$  as a constant of rate;  $P$  is the number of individuals per grid;  $\phi$  is a conversion coefficient between carbon content (g) and biomass ( $\mu g$ ), valued at 0.5; 28.5 ( $\mu g/\mu mol$ ) is a  $CO_2$  - biomass conversion coefficient;  $FPC$  represents the foliage projective cover;  $C_{tissue}$  is the carbon content of organ (g);  $cn_{tissue}$  ( $gC/gN$ ) is the mass ratios equal to 29, 330, and 29 respectively.

Table 2. Major process and mechanism of canopy fluxes.

Major processes	Mechanism
Biogeophysics	On account of canopy energy balance, calculate (1) sensible heat, latent heat and momentum roughness index of the surface and plant; (2) diffuse radiation fluxes of the surface and plant; (3) humidity of the surface
Temperature and pressure derivation	Describe responses of pressure and relative humidity to the temperature
Monin ObukIni	Calculate Monin-Obukhov length and wind velocity in stability based on Monin-Obukhov theory
Friction Velocity	Describe the profile of wind velocity, temperature and humidity on the surface
Fraction wetdry	Calculate the proportions of dry and wet leaves
Energy transfer	Simulate energy transferring in the canopy with the two-stream method
Surface Radiation	Calculate absorbed radiation by the plant and surface as well as photosynthesis active radiation of sunlit and shaded leaf on account of energy balance rule
Canopy flux	Calculate aero-dynamical resistance, temperature, humidity and leaf boundary impedance to describe energy and water vapor flux among atmosphere, canopy air area, foliage and ground.

$g(T)$  is a function of temperature:

$$g(T) = e^{308.56 \left( \frac{1}{56.02 + t_{soir}} - \frac{1}{-227.13} \right)} \quad (6)$$

where  $t_{soir}$  is the temperature of rhizospheric area.

#### 4) Net primary productivity (NPP)

Dry biomass increment ( $\Delta m$ ) is set as photosynthesis rate minus respiration one for calculating net primary productivity (NPP, KgC/m<sup>2</sup>). Due to the sunshine hour as the important factor of daily photosynthesis, it is added to the derivation for improving the calculation method.

$$\Delta m = 28.5 \left( \frac{\Delta h}{24} \times A - R_a \right) \times 86400 \quad (7)$$

$$NPP = \Delta m \times 0.5 \times 10^{-6} \quad (8)$$

where  $\Delta h$  is the sunshine hour per grid; 28.5 ( $\mu/\mu mol$ ) is a CO<sub>2</sub> – biomass conversion factor;  $0.5 \times 10^{-6}$  is the conversion coefficient from biomass to carbon content ( $\mu g/g$ ).

#### 5) Allocation

Based on the allocation process in CLM-DGVM, this model is determined assuming three basic allometric relationships, i.e., “pipe model” theory, the proportional relationship between leaf and root mass and that between height and top crown area [61-64], to allocate biomass to tree leaves, sapwood, and roots ( $C_{leaf}$ ,  $C_{sapwood}$ ,  $C_{root}$ ).

Firstly, it is assumed that the biomass increment is only allocated between leaf and root:

$$\text{Biomass increment: } \Delta m = \Delta C_{leaf} + \Delta C_{root} \quad (9)$$

$$\text{Assuming: } k_{lntorm} = lr_{max} \omega \quad (10)$$

$$\text{Then } \Delta C_{root} = (C_{leaf} + \Delta C_{leaf}) / k_{lntorm} - C_{root} \quad (11)$$

Biomass increment of the leaf:

$$\Delta C_{leaf} = \frac{\Delta m - C_{leaf} / k_{lntorm} + C_{root}}{1 + 1 / k_{lntorm}} \quad (12)$$

where  $k_{lntorm}$ , represents the ratio of leaf mass to root mass;  $lr_{max}$ , is the ratio of leaf mass to root mass without soil water content constraint (Table 3);  $\omega$  is the ratio of actual photosynthesis to potential one during 10d.

On account of three hypotheses and assumptions above, the function of leaf biomass increment will be obtained with related parameters, such as wood density, volume and diameter of the stem.  $\Delta C_{leaf}$  is set as the argument and  $f(\Delta C_{leaf})$  as the dependent variable.  $\Delta C_{leaf}$  could be solved with Bisection method to update leaf biomass.

$$f(\Delta C_{leaf}) = k_{allom2}^{\frac{2}{k_{allom3}}} \cdot \frac{C_{sapwood} + \Delta m - \Delta C_{leaf} - (C_{leaf} + \Delta C_{leaf}) / k_{lntorm} + C_{root} + C_{heart}}{\frac{1}{4} \Pi} - C_{sapwood} + \Delta m - \Delta C_{leaf} - \left[ \frac{(C_{leaf} + \Delta C_{leaf}) / k_{lntorm} + C_{root}}{(C_{leaf} + \Delta C_{leaf}) \cdot SLA \cdot \rho_{woddens} / k_{latosa}} \right]^{1 + \frac{1}{2k_{allom3}}} \quad (13)$$

where allometric parameter  $k_{allom2} = 40$ ,  $k_{allom3} = 0.5$ ;  $k_{latosa}$  is the ratio of leaf area to sapwood cross-sectional area, valued at 8,000;  $\Pi = 3.14159$ ;  $SLA$  ( $m^2/g$ ) is specific leaf area;  $\rho_{woddens}$  ( $g/m^2$ ) is the wood density, valued at  $2.0 \times 10^5$ .

The calculation equation of  $SLA$  [55-66] is shown as follows:

$$SLA = 2 \times 10^{-4} \cdot \frac{e^{6.15}}{(12a_{leaf})^{0.46}} \quad (14)$$

Table 3. Parameters dependent on plant function types.

Parameters	Unit	Temperate needle-leaf evergreen tree	Temperate broadleaf deciduous tree	Boreal needle- leaf evergreen tree	Grasses	Crops
Subordinate index of respiration ( $r$ )	$gC/gN$	1.2	1.2	0.6	0.6	0.6
Lifespan of leaf ( $lt\_lon$ )	$yr$	2	1	2	1	1
Lifespan of sapwood ( $st\_lon$ )	$yr$	20	20	20	1	1
Lifespan of root ( $rt\_lon$ )	$yr$	2	2	2	2	2
Transferred index of leaf and root ( $lr_{max}$ )	-	1	1	1	0.75	0.75
Live leaf Lifespan ( $a_{leaf}$ )	$yr$	2	0.5	2	1	1
Maximum mortality ( $k_{mort}$ )	$/yr$	1	1	3	-	-
Turnover index of leaf ( $turn_{pl}$ )	-	25	185	51.5	285	1100
Turnover index of sapwood ( $turn_{ps}$ )	-	25	82.5	50	285	1100
Turnover index of root ( $turn_{pr}$ )	-	25	42.5	50	-	1100
Adjustment index of soil decomposition ( $sol_k$ )	-	1.75	3.2	1.75	1.88	0.8

where  $a_{leaf}$  represents the live leaf lifespan (Table 3).

#### 6) Turnover

According to the lifespan of leaf, sapwood and root in different plant function types, total carbon fixation from above litter to the below could be derived as well as total biomass from sapwood to heartwood. The total turnover biomass ( $\Delta C_{turn}$ ) is calculated as follows:

$$\Delta C_{turn} = \sum C_{tissue} f_{tissue} \quad (15)$$

where  $f_{tissue}$  represents the number of carbon turnover in tissues, or the inverse of tissue lifespan, i.e.,  $lt\_lon$ ,  $st\_lon$  and  $rt\_lon$  (Table 3).

With the decrease of tissue turnover,  $C_{tissue}$  will also be changed, of which the derivation is shown as followed:

$$\Delta C_{leaf} = C_{leaf} f_{leaf} / turn_{pl} \quad (16)$$

$$\Delta C_{sapwood} = C_{sapwood} f_{sapwood} / turn_{ps} \quad (17)$$

$$\Delta C_{root} = C_{root} f_{root} / turn_{pr} \quad (18)$$

Because the simulation time is 10d, it is required to adjust the turnover index, including those of leaf, sapwood and root ( $turn_{pl}$ ,  $turn_{ps}$  and  $turn_{pr}$ ) (Table 3).

The sapwood ( $C_{sapwood}$ ) turns into the heartwood ( $C_{heartwood}$ ) while leaves and roots change into the surface and subsurface litters ( $C_{L,ag}$ ,  $C_{L,bg}$ ):

$$\Delta C_{heartwood} = C_{sapwood} f_{sapwood} \quad (19)$$

$$\Delta C_{L,ag} = C_{leaf} f_{leaf} P \quad (20)$$

$$\Delta C_{L,bg} = C_{root} f_{root} P \quad (21)$$

#### 7) Recruitment of new individuals

On the recruitment of new individuals, two methods are applied for the natural and artificial plant. Confined by the environment and resources, the natural growth trend of plant population is often accordance with the logistic growth parabola. So, Logistics Model is applied in the model for the evolution of natural species richness. Then, the number could be derived. However, affected by human being activities, artificial forest and crops are increasing while the natural plants decreasing in Luanhe basin. As a result, with the local forest and land use information, the individual number per square meter of different plant types could be updated for several years.

#### 8) Mortality

In the light of growth mechanisms of different plants, the defoliation is generalized as the forced process except for evergreen in this model. It is indicated that all leaf biomass is shifted to the carbon pool above litter in a certain month (Table 4).

During the process, the total mortality ( $mort$ ) refers to the sum of natural and heat-stress one ( $mort_{graff}$ ,  $mort_{heat}$ ) as a comprehensive function of 10-day growing degree days, asymptotic maximum mortality rate ( $k_{mort}$ ) and growth efficiency ( $k_{mort2}$ ), related to carbon-turnover flux. Then, the population in the grid will be updated:

$$P = P - P \cdot mort \quad (22)$$

Table 4. Defoliation time of deciduous plants.

Plant types	Initial time
Temperate broadleaf deciduous tree	December
Boreal deciduous	November
Grasses	November
Crops	November

9) Decomposition

Litters are decomposed into organic matters by themselves and soil heterotrophic respiration. It is assumed that there are carbon pools for fast and slow decomposition, of which the rate is influenced by soil temperature, water content and time. The 70% decomposed carbon flux will be released into atmosphere while others will stay in the soil; The 98.5% of the latter will reach pools with fast decomposition while others in slow pools [67]. Thus, the total carbon flux from soil to atmosphere will be obtained to update fast and slow soil carbon pool as well as heterotrophic respiration.

Because the temperature and humidity are significant factors of litters and soil carbon pools, it is necessary to identify their efficient coefficient ( $W_{res}, T_{res}$ ) to update decomposition parameters of litters and fast/slow carbon pool. The calculated process is the same to CLM-DGVM, so it is no need to discuss details.

Decomposed index of litters:

$$k_l = 0.5 \times T_{res} \times W_{res} \times \Delta d \times solk \quad (23)$$

Decomposed index of fast pool:

$$k_{l-f} = 0.03 \times T_{res} \times W_{res} \times \Delta d \times solk \quad (24)$$

Decomposed index of slow pool:

$$k_{l-l} = 0.001 \times T_{res} \times W_{res} \times \Delta d \times solk \quad (25)$$

where  $\Delta d$  is the simulated time step, set as 10d.

Carbon content in litters and soil carbon pool is calculated by attenuation equation as follows:

$$C = C_0(1 - e^{-k}) \quad (26)$$

where  $C$  represents the carbon content;  $C_0$  is the initial value;  $k$  is the decomposed index; the decomposition adjustment coefficient of soil ( $solk$ ) is added because of the soil-decomposition heterogeneity for different plants (Table 3).

If  $C_0$  in Equation (26) is replaced by the initial carbon content of litters, fast and slow soil pools respectively, the updated carbon content in the corresponding pools can be obtained by substituting Equation (23), (24) and (25) in Equation (26).

Comparison

Because of the large spatial scale, different ecosystems and the whole basin with the average leaf area index are variable, constrained by the distribution and spatial-temporal discontinuity. The sequential field data for the whole basin is so absent that it is necessary to compare LAI from the remote-sensing images with simulated value. For Luanhe Basin, coupled with topography and plant distribution, the comparison is implemented with the strategy on combination of whole basin and typical regions.

1) The whole basin

Annual LAI is derived from the remote-sensing images of MODIS in 2005, 2006 and 2010 on the International Scientific Data Service Platform to compare with the simulated results, of which the resolution is 500 m×500 m after interpolation. Results show that the relative error between both results in 2005 and 2006 is 36% and 32% respectively, but that in 2010 is slightly greater as about 39%. Owing to spatial heterogeneity reduced by average verification of the whole basin, the representativeness is not convinced completely. As a result, comparison of typical regions is required.

2) Typical regions

The highland meadows in upper reaches, mountainous forests in middle reaches and farmland on the plain in lower reaches were selected for comparison of typical regions. To meet the accuracy for typical regions, LAI with 30 m×30 m is implemented from LANDSAT-5 remote sensing. In general, results of typical regions are relatively fine except for those of farmland in lower reaches in September 2005 (Table 5, Fig. 6). It is required that the simulation of cultivated plant should be improved especially for economic and field crops because of lower reaches occupied by tilled land and tidal flat.

Sensitivity Analysis

The terrestrial carbon cycle model is a simple and abstract generalization on the evolution and status changes in multiple spatial-temporal scale of plant, soil and other research objects in ecology. As a result, the uncertainty will be produced, i.e., the deviation between simulation and real value. Meanwhile, any model is unable to suit regions with different spatial and temporal scales. Thus, partial input parameters should be adjusted on account of research scale. Currently, the input data of carbon cycle model consists of meteorological, soil and plant data, derived from monitoring station, remote-sensing images and field experiment. Due to its diversity, a sensitivity analysis on input data is required to identify influences of input data on the results quantitatively. In the model, input parameters with influences on results are mainly involved with leaf area index, foliage projective coverage, direct radiation, diffuse radiation, atmospheric pressure, surface

Table 5. Compared results on LAI in typical regions of Luanhe Basin.

Date	Location	Average of remote sense	Average of simulated results	Relative errors (%)
1995/9/20	Mid-lower reaches	3.16	2.63	16.77%
2005/9/10	Lower reaches	3.81	5.41	41.99%
2006/7/21	Middle reaches	5.8	4.07	29.83%
2007/6/10	Upper reaches	1.56	1.73	10.90%

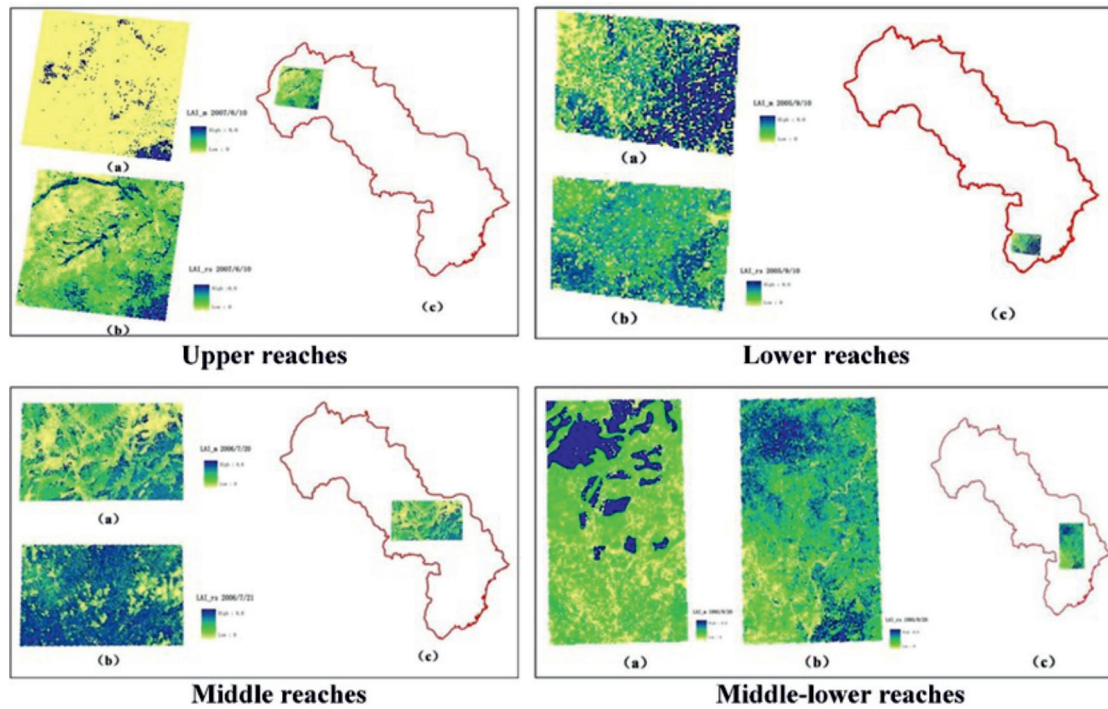


Fig. 6. Comparison figure on LAI simulation and remote-sensing retrieval in upper reaches, middle reaches, middle-lower reaches and lower reaches: a) simulated results; b) remote-sensing extraction; c) location in the basin.

temperature, wind velocity, actual sunshine hours, humidity and volumetric water content of soil. Net primary productivity and leaf area index are selected as the verified parameters, because micro-process on stoma (including photosynthesis and respiration) and macro-process on vegetation succession could be characterized by the both respectively. Those input values are increased or decreased by 10% to test the sensitivity of the model, the maximum of which will be the result in the process.

$$IC = \max [IC_{+10\%}, IC_{-10\%}] \tag{27}$$

$$IC_{+10\%} = 100 \times \frac{|res_{+10\%} - res_{no}|}{res_{no}} \tag{28}$$

$$IC_{-10\%} = 100 \times \frac{|res_{-10\%} - res_{no}|}{res_{no}} \tag{29}$$

where  $IC_{+10\%}$  and  $IC_{-10\%}$  (%) represent the change amplitude of output results when input values are increased or decreased by 10% respectively;  $res_{+10\%}$  and  $res_{-10\%}$  represent output results when input values are increased or decreased by 10% respectively;  $res_{no}$  represents output results without changes.

In general, surface humidity becomes the most influential input parameter of RTCCM-3S in Luanhe Basin, of which  $NPP$  and LAI change by more than 30%. For  $NPP$ , surface humidity, atmospheric pressure and diffuse radiation seem to be the most major factors causing the results changing by more than 10%. The two former ones are relative with the leaf stoma behavior and the latter could influence the light-limited rate. Actual sunshine hours, direct radiation and initial LAI lead to results changing by 5%-10%. Initial foliage projective cover and volumetric water content of soil cause changes by 1%-2%. Wind velocity has little influence with the change amplitude only at 0.08%. For LAI, surface humidity and atmospheric pressure are

Table 6. Results on sensitivity analysis of RTCCM-3S in Luanhe Basin.

Input parameter	Amplitude of <i>NPP</i> (%)	Amplitude of LAI (%)
Initial LAI	6.74	6.11
Initial foliage Projective cover	1.42	7.38
Diffuse radiation	15.25	7.38
Direct radiation	8.68	4.31
Atmospheric pressure	20.63	10.07
Surface temperature	11.11	6.47
Wind velocity	0.08	0.00
Actual sunshine hours	8.71	4.28
Surface humidity	57.64	32.81
Volumetric soil water content	1.13	0.52

the most major input values causing the results changing by more than 10%. Changes are not prominent because of variation in diffuse and direct radiation, initial foliage projective cover, initial LAI, surface temperature and actual sunshine hours. Those in volumetric water content of soil and wind speed have little influence on the results (Table 6).

### Results

In the view of carbon cycle mechanism, *NPP*, LAI, surface and subsurface biomass, carbon content of the soil are chosen to analyze and discuss the regional carbon cycle evolution. The initial year of simulation is 1992. The results of the first three years are not considered in results and discussions, because it is the warm-up period.

### Net Primary Productivity (*NPP*)

Annual *NPP* in Luanhe Basin from 1995 to 2010 was about 0.18 KgC/m<sup>2</sup>. Its inter-annual change showed a minor fluctuation with an insignificant increase (Fig. 7a). Compared with 1995, it grew by 20.67%. In terms of spatial distribution, *NPP* shows obvious regional differences (Fig. 7b). In the whole basin, the high values were concentrated at the mountains in middle-upper reaches and the plains in the lower reaches, the *NPP* reaches a maximum of 2.22 KgC/m<sup>2</sup>. In this area, the artificial vegetation cover showed a higher degree than in the grasses and coastal beaches.

### Leaf Area Index (LAI)

Annual LAI in Luanhe Basin from 1995 to 2010 was 1.45, of which inter-annual change showed a certain fluctuation with a minor “jumped” increase, but not significant. Compared with 1995, LAI in 2010 increased by 5.8% (Fig. 8a). The spatial distribution characteristics of LAI are similar to those of *NPP* because it was influenced by initial value and *NPP* greatly (Fig. 8b). In the view of whole basin, high-value zones occurred in the regions with higher degree of vegetation cover.

### Carbon Content in Surface and Subsurface Litters

Annual carbon content in surface and subsurface litter per area during 1995-2010 was 0.1458 g/m<sup>2</sup> and 0.0056 g/m<sup>2</sup> respectively, with no significant change trend. Compared with 1995, the former decreased by 4.17% while the latter increased by 1.28% in 2010 (Fig. 9(a, b)). It was indicated that the carbon in surface litter was transferred to subsurface continuously. However, the effect was not obvious because of limited temporal scale. In the view of spatial distribution in the whole basin, carbon contents in surface and subsurface litters shows obvious regional differences, carbon

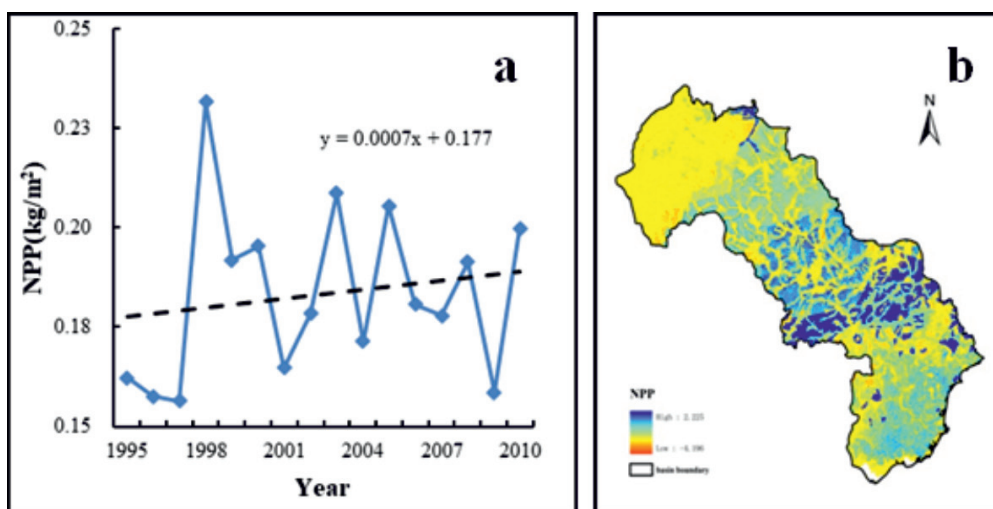


Fig. 7. Evolution and spatial distribution of annual *NPP* per during 1995-2010: a) evolution; b) spatial distribution.

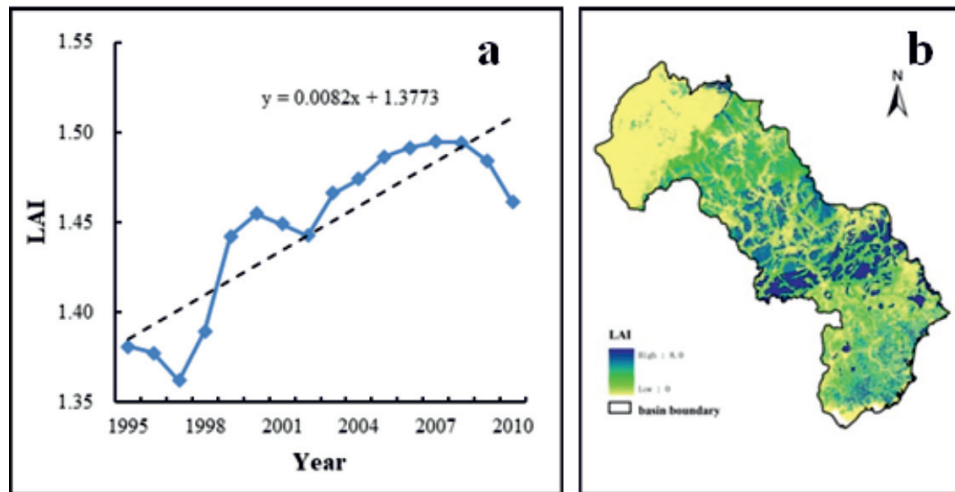


Fig. 8. Inter-annual evolution and spatial distribution of LAI during 1995-2010: a) inter-annual evolution; b) spatial distribution.

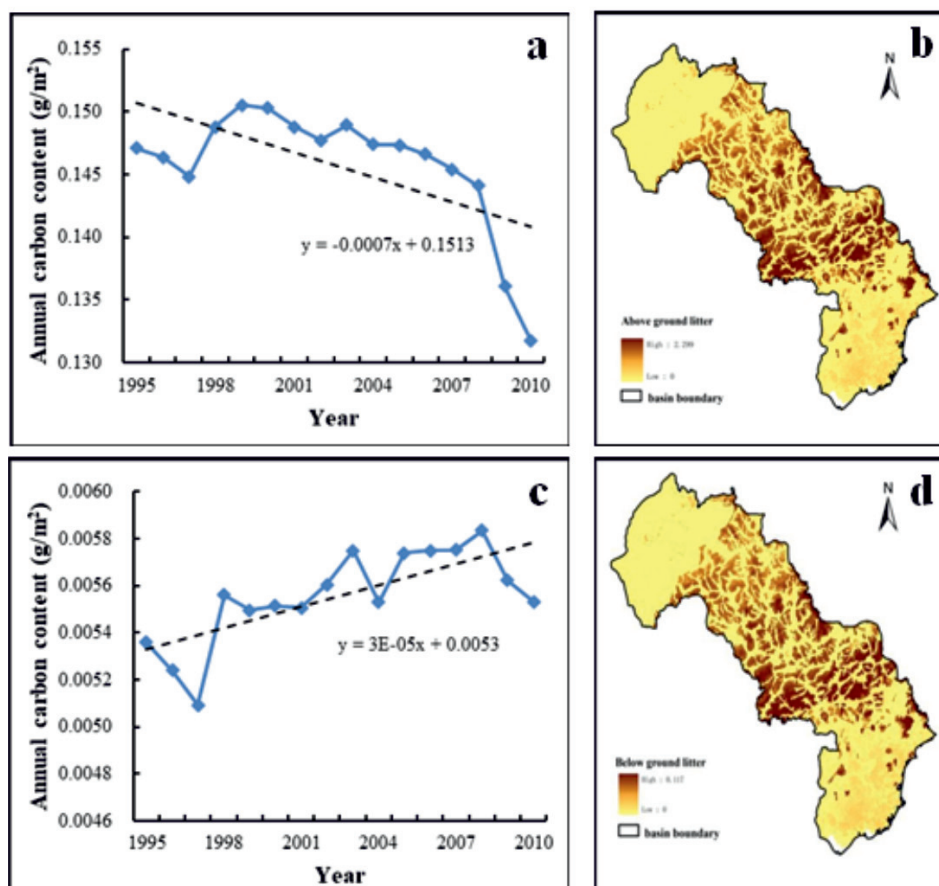


Fig. 9. Annual carbon content and spatial distribution in surface litters and subsurface litters during 1995-2010: a) annual carbon content in surface litters; b) spatial distribution in surface litters; c) annual carbon content in subsurface litters; d) spatial distribution in subsurface litters.

contents in surface and subsurface litters of middle-upper reaches were larger than those in other regions (Fig. 9(c,d)). However, carbon content was lower in lower reaches dominated by artificial plant cover, mainly due to the disturbance of human activities on the natural succession of ecosystem.

#### Soil Carbon Content

Daily carbon content per soil area in Luanhe Basin during 1995-2010 was about 0.0115 g/m<sup>2</sup>, without prominent inter-annual changes. Compared with 1995, it was decreased by 4.8% (Fig. 10a). In the whole basin,

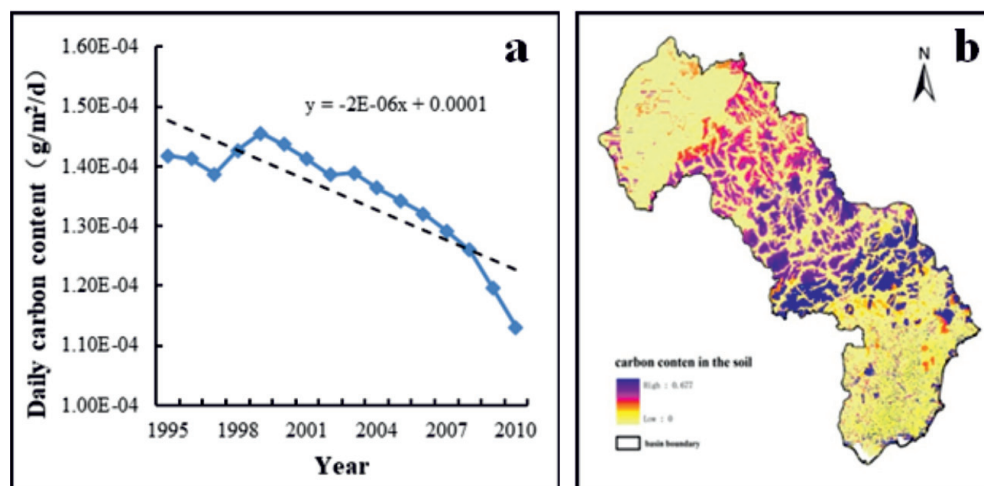


Fig. 10. Daily carbon content and spatial distribution of annual carbon content of soil during 1995-2010: a) daily carbon content; b) spatial distribution of annual carbon content (KgC).

its spatial distribution indicated that the carbon content was higher in middle-upper reaches, it shows obvious regional differences (Fig. 10b). There existed “patchy” high-value areas in low-value zones of lower reaches. The soil carbon content in the upstream low-value area is higher than that in the surface and subsurface litters. It is also reflected that cultivation, urbanization and other human activities have influences on plants and soil in the ecosystem.

## Discussion

### Analysis about the Change of *NPP* and LAI

The *NPP* and LAI in the Luanhe River Basin show significant zonal characteristics, and related studies have shown that meteorological and topographical factors are the key factors affecting them [68]. Meteorological factors act on plant growth and distribution through temperature changes and precipitation mechanisms, affecting plant photosynthesis and respiration to change vegetation *NPP* and LAI [69-70]. Liu et al. found that the joint effect of air temperature and precipitation on *NPP* and LAI was 25.13% higher than the individual effect [71]. Differences in hydrothermal and soil conditions at different elevations affect regional vegetation patterns, which in turn cause changes in vegetation *NPP* and LAI [72]. This study found that the *NPP* and LAI values were greater within the altitude range of 200 m-1200 m than those at altitudes higher than 1200m or less than 200 m. The altitude range of 200-1200 m is located in the middle reaches of the Luanhe Basin, which belongs to the Beijing-Tianjin Water Containment Ecological Function Protection Zone [73]. The land cover in this area is mostly forest, and the *NPP* and LAI are fluctuating and slowly decreasing. The altitude higher than 1200m is the mountainous area in the

upper reaches of the watershed, and the main types are meadow and cultivated land. The ecological sensitivity and vulnerability of this area are high due to soil sanding problems caused by overgrazing, and *NPP* and LAI decrease rapidly with the increase of altitude [74].

In addition, various input parameters of the model have a significant impact on *NPP* and LAI, such as vegetation type parameters, soil parameters, and crop anisotropic growth parameters [75]. Due to the surface temperature, humidity, soil types and other factors, different ecological changes will come up in different geographic areas with the same plant type on which the same parameters are employed, e.g. intra- and inter-annual evolution of temperate broadleaf deciduous trees in the mountainous area is different from ones in the plain [76]. As a result, plant types and its key model parameters should be detailed to expand application. Meanwhile, input data involved with soil are only “static” values, such as volumetric soil water content, porosity and other textural characteristics, which should be updated seasonally and annually. Because of the space-time distribution of water resources, especially for the precipitation and water usage from the surface and subsurface, soil water content could be one of the most sensitive values for the evapotranspiration, which will have an indirect effect on the *NPP* and LAI with stomata action [77]. In a word, input data of soil will be dynamic if measurement results are derived. In the Luanhe Basin, growth process and distribution of grasses and artificial crops are disturbed by human-being activity. It is necessary to improve biomass increment allocation of grasses and artificial crops. Detailed classification is required for the latter because it involves with fruit trees, the corn, winter wheat and others. Some relative biological properties and phenological characteristics of them are diverse, such as the average height, the maximum apical cap, leaf length and defoliation time. All values above play major roles

in the allometric process. It is necessary to increase *NPP* and *LAI* of the grass according to adjusting the key allometric parameters with recent distribution [78].

### Analysis about the Change of Carbon Content

This study found that the carbon in the surface litter in the Luanhe Basin was continuously transferred the subsurface litter, but the soil carbon content showed a decreasing trend. In terms of spatial distribution, the characteristics of both are similar to those of the *NPP* and *LAI*, and both show significant regional differences. Litters is the main source of soil carbon, and it can regulate the dynamic balance of soil carbon content [79]. The altitude range of 200-1200 m is the forest zone with good vegetation coverage. Vegetation litter mainly accumulates on the soil surface. Environmental factors such as temperature and humidity on the soil surface will accelerate the decomposition of litter. Decomposition products first accumulate on the surface. With the accumulation of humus, the decomposition products are transported to the deep soil, forming the phenomenon that the carbon in the surface litter is continuously transferred to the subsurface litter [80-81]. In the meadow area with altitude higher than 1200 m, 92% of the organic matter in the grassland will be distributed to the underground roots through photosynthesis [26, 82]. In addition, herbs are basically annuals, and a large number of roots died in that year and entered the carbon cycle, thereby increasing soil carbon content [82]. In this paper, the soil carbon content in this area is higher than that in the surface and subsurface litters. The downstream plain areas with altitude less than 200 m are mostly cultivated land and construction land types with high degree of human activities, resulting in lower carbon content in surface and subsurface litters. The difference is that there are "patches" high value areas of soil carbon content in the region. This phenomenon arises from the different farming methods on the cultivated land. Adopting no-till will increase the soil carbon content by increasing the protection of soil aggregates and delaying the rate of organic matter decomposition. In contrast, long-term conventional tillage breaks the good soil structure, organic carbon is exposed to air without protection, the rate of mineralization is accelerated, and soil carbon content is reduced [83].

### Conclusions

The 3S-based regional terrestrial carbon cycle model in Luanhe Basin is constructed with component-based development strategy to simulate and identify carbon cycle evolution of terrestrial ecosystems during 1995-2010, combining measured weather data, prototype observation data of soil and plants as well as remote-sensing information in different spatial and

temporal scales. The model has the ability of describing canopy fluxes, net primary productivity, biomass allocation and turnover, mortality, decomposition of soil organic matter and other dynamic processes. It adds the recruitment of new individuals and forced defoliation process. The main conclusions are as follows:

1) The sequential field data for the whole basin is so absent that it is necessary to compare *LAI* from the remote-sensing images with simulated value for the whole area and typical district. Results indicate that relative errors are less than 40% in Luanhe Basin.

2) To identify effects of input data on simulated results, a sensitivity analysis is implemented. It is shown that the most influential input parameter is surface humidity, and the change amplitudes of *NPP* and *LAI* are up to 30% above, followed by atmospheric pressure and diffuse radiation with change amplitudes greater than 10%.

3) The carbon cycle evolution in Luanhe Basin from 1995 to 2010 is simulated and analyzed and the rules are shown as followed. In the temporal scale, the inter-annual change of *LAI* with a slight growth trend is larger than that of *NPP*, carbon content in surface and subsurface litters, soil carbon content. There are obvious regional differences in spatial view. The spatial distribution of results are consistent with watershed plant and soil, displaying the characteristics that the above major variables in mountainous regions of upper and middle reaches are greater than those of grassland meadows in upper reaches and plains in lower reaches.

In the future, field experiment should be done for the verification. There are three major reasons for field experiment in the future. On one hand, The sequential field data for all plant function types in different geographical areas of the basin is need for the verification to improve simulated accuracy of the model, including the *LAI* and biomass of tissues(leaf, sapwood, heartwood and root). On the other hand, key parameters of plant function types on the process of allometry and mortality should be adjusted by the long-term field data. Finally, under the ground of climate changes, it is helpful to identify the driving mechanism of carbon cycle.

The model is not only helpful to understand spatial-temporal evolution of terrestrial ecosystem, but also will become one of key technologies on comprehensive response to global climate changes, migrating regional effects of eco-environmental problems and constructing low-carbon and environment-friendly society.

### Acknowledgments

This research was supported by the Five Major Excellent Talent Programs of IWHR (WR0199A012021), the National Science Fund Project (Grant No. 52130907) and the National Science Fund for Young Scholars (Grant No. 52109043).

### Conflict of Interest

The authors declare no conflict of interest.

### References

- PRINCIOTTA F. Global Climate Change and the Mitigation Challenge. *J Air Waste Manag Assoc*, **59** (10), 1194, **2009**.
- LONNGREN K.E., BAI E.W. On the global warming problem due to carbon dioxide. *Energ Policy*, **36** (4), 1567, **2008**.
- CETIN M. A Change in the Amount of CO<sub>2</sub> at the Center of the Examination Halls: Case Study of Turkey. *Studies on Ethno-Medicine*, **10** (2), 146, **2016**.
- SERT E.B., TURKMEN M., CETIN M. Heavy metal accumulation in rosemary leaves and stems exposed to traffic-related pollution near Adana-İskenderun Highway (Hatay, Turkey). *Environ Monit Assess*, **191**, 553, **2019**.
- WU C.Y., ZHANG X.Y., GUO L.F., ZHONG J.T., WANG D.Y., MIAO C.H., GAO, X., ZHANG X.L. An inversion model based on GEOS-Chem for estimating global and China's terrestrial carbon fluxes in 2019. *ACCR*, **14** (1), 49, **2023**.
- IPCC (Intergovernmental Panel on Climate Change). *Climate change 2021: The physical science basis. Contribution to the sixth assessment report of the intergovernmental panel on climate change*. Cambridge University Press, **2021**.
- QU Q., XU H.W., AI Z., WANG M.G., WANG G.L., LIU G.B., GEISSEN V., RITSEMA C.J., XUE S. Impacts of extreme weather events on terrestrial carbon and nitrogen cycling: A global meta-analysis. *Environ Pollut*, **319**, 120996, **2023**.
- THAKUR M.P., RISCH A.C., PUTTEN W.H.V.D. Biotic responses to climate extremes in terrestrial ecosystems. *iScience*, **25** (7), 104559, **2022**.
- CETIN M. Sustainability of urban coastal area management: A case study on Cide, *J Sustain Forest*, **35** (7), 527, **2016**.
- BARNES D.K.A., SANDS C.J., PAULSEN M.L., MORENO B., MOREAU C., HELD C., DOWNEY R., BAX N., STARK J.S., ZWERSCHKE N. Societal importance of Antarctic negative feedbacks on climate change: blue carbon gains from sea ice, ice shelf and glacier losses. *Sci Nat*, **108**, 43, **2021**.
- CETIN M. Using GIS analysis to assess urban green space in terms of accessibility: case study in Kutahya. *Int J Sust Dev World*, **22** (5), 420, **2015**.
- GUO K., ZHANG X.C., LIU J.M., WU, Z.F., CHEN M., ZHANG K.X., CHEN, Y.Y. Establishment of an integrated decision-making method for planning the ecological restoration of terrestrial ecosystems. *Sci Total Environ*, **741**, 139852, **2020**.
- ZHANG Q., KONG D., SHI P., SINGH V.P., SUN P. Vegetation phenology on the Qinghai-Tibetan Plateau and its response to climate change (1982-2013). *Agric For Meteorol*, **248**, 408, **2018**.
- TOAN T.L., QUEGAN S., DAVIDSON M.W.J., BALZTER H., PAILLOU P., PAPATHANASSIOU K., PLUMMER S., ROCCA F., SAATCHI S., SHUGART H., ULANDER L. The BIOMASS mission: Mapping global forest biomass to better understand the terrestrial carbon cycle. *Remote Sens Environ*, **115** (11), 2850, **2011**.
- QI J.Y., DU X.Z., ZHANG X.S., LEE S.C., WU Y.P., DENG J., MOGLEN G.E., SADEGHI A.M., MCCARTY G.W. Modeling riverine dissolved and particulate organic carbon fluxes from two small watersheds in the northeastern United States. *Environ Modell Softw.*, **124**, 104601, **2020**.
- ZENG S.D., XIA J., CHEN X.D., ZOU L., DU H., SHE D.X. Integrated land-surface hydrological and biogeochemical processes in simulating water, energy and carbon fluxes over two different ecosystems. *J Hydrol*, **582**, 124390, **2020**.
- WANI O.A., KUMAR S., HUSSAIN N., WANI A.L.A., BABU S., ALAM P., RASHID M., POPESCU S.M., MANSOOR S. Multi-scale processes influencing global carbon storage and land-carbon-climate nexus: A critical review. *Pedosphere*, **5**, **2022**.
- POULTER B., FRANK D.C., HODSON E.L., ZIMMERMANN N.E. Impacts of land cover and climate data selection on understanding terrestrial carbon dynamics and the CO<sub>2</sub> airborne fraction. *Biogeosciences*, **8** (8), 2027, **2011**.
- WEN Y.Y., LIU X.P., BAI Y., SUN Y., YANG J., LIN K., PEI F.S., YAN Y.C. Determining the impacts of climate change and urban expansion on terrestrial net primary production in China. *JEM*, **240**, 75, **2019**.
- CETIN M. *Landscape Engineering, Protecting Soil, and Runoff Storm Water*. *Advances in Landscape Architecture*, 27<sup>th</sup> ed.; MURAT ÖZYAVUZ., IntechOpen: Rijeka, Croatia, 698, **2013**.
- HEAD M., BERNIER P., LEVASSEUR A., BEAUREGARD R., MARGNI M. Forestry carbon budget models to improve biogenic carbon accounting in life cycle assessment. *J Clean Prod*, **213**, 289, **2019**.
- ZHU H.Y., ZHANG D.D., GOH H.H., WANG S.Y., AHMAD T., MAO D.J.F., LIU T.H., ZHAO H.S., WU T. Future data center energy-conservation and emission-reduction technologies in the context of smart and low-carbon city construction. *Sustain Cities Soc*, **89**, 104322, **2023**.
- KONG R., ZHANG Z.X., ZHANG F.Y., TIAN J.X., CHANG J., JIANG S.S., ZHU B., CHEN X. Increasing carbon storage in subtropical forests over the Yangtze River basin and its relations to the major ecological projects. *Sci Total Environ*, **709**, 136163, **2020**.
- CICEK N., ERDOGAN M., YUCEDAG C., CETIN M. Improving the Detrimental Aspects of Salinity in Salinized Soils of Arid and Semi-arid Areas for Effects of Vermicompost Leachate on Salt Stress in Seedlings. *Water Air Soil Poll*, **233**, 197, **2022**.
- SRINET R., NANDY S., PATEL N.R., PADALIA H., WATHAM T., SINGH S.K., CHAUHAN P. Simulation of forest carbon fluxes by integrating remote sensing data into biome-BGC model. *Ecol Model*, **475**, 110185, **2023**.
- UMAIR M., KIM D., RAY R.L., CHOI M. Evaluation of atmospheric and terrestrial effects in the carbon cycle for forest and grassland ecosystems using a remote sensing and modeling approach. *Agric For Meteorol*, **295**, 108187, **2020**.
- CETIN M., PEKKAN O.L., OZTURK G.B., KRUKCUOGLU M.A.S., KUCUKPEHLIVAN T., CABUK A. Examination of the Change in the Vegetation Around the Kirka Boron Mine Site by Using Remote Sensing Techniques. *Water Air Soil Poll*, **233**, 254, **2022**.
- GAO Y., JIA J.J., LU Y., YANG T.T., LYU S., SHI K., ZHOU F., YU G.R. Determining dominating control mechanisms of inland water carbon cycling processes and

- associated gross primary productivity on regional and global scales. *Earth-Sci Rev*, **213**, 103497, **2021**.
29. CHENG K.Y., RILEY W.J., KEENAN T.F. Hourly water-carbon interactions modulate decadal water-use efficiency trends inferred from ecosystem-scale measurements. *Agric For Meteorol*, **326** (15), 109158, **2022**.
  30. LIU Y., JU W., HE H., WANG S., SUN R., ZHANG Y. Changes of net primary productivity in China during recent 11 years detected using an ecological model driven by MODIS data. *Front Earth Sci*, **7** (1), 112, **2013**.
  31. LINDESKOG M., LAGERGREN F., SMITH B., RAMMIG A. Accounting for forest management in the estimation of forest carbon balance using the dynamic vegetation model LPJ-GUESS (v4.0, r9333): Implementation and evaluation of simulations for Europe. *Geosci Model Dev*, **14**, 6071, **2021**.
  32. TONG X., BRANDT M., YUE Y., HORION S., WANG K., KEERSMAECKER W.D., TIAN F., SCHURGERS G., XIAO X., LUO Y., CHEN C., MYNENI R., SHI Z., CHEN H., FENSHOLT R. Increased vegetation growth and carbon stock in China karst via ecological engineering. *Nat Sustain*, **1** (1), 44, **2018**.
  33. CRAIG H. The natural distribution of radiocarbon and the ex-change time of carbon dioxide between atmosphere and sea. *Tellus Journal*, **9**, 1, **1957**.
  34. SUN G.D., MU M. Role of hydrological parameters in the uncertainty in modeled soil organic carbon using a coupled water-carbon cycle model. *Ecol Complex*, **50**, 100986, **2022**.
  35. OGUTU B.O., D'ADAMO F., DASH J. Impact of vegetation greening on carbon and water cycle in the African Sahel-Sudano-Guinean region. *Global Planet Change*, **202**, 103524, **2021**.
  36. KNOWLES J.F., SCOTT R.L., MINOR R.L., BARRON-GAFFORD G.A. Ecosystem carbon and water cycling from a sky island montane forest. *Agric For Meteorol*, **281**, 107835, **2020**.
  37. GANG C.C., ZHANG Y.Z., WANG Z.Q., CHEN Y.Z., YANG Y., LI J.L., CHENG J.M., QI J.G., ODEN I. Modeling the dynamics of distribution, extent, and NPP of global terrestrial ecosystems in response to future climate change. *Global Planet Change*, **148**, 153, **2017**.
  38. AYTEN E., KAMIL E., DAVUT A., FATIH E. Modeling Impacts of Land Uses on Carbon and Nitrogen Contents, Carbon Dioxide and Water Effluxes of Mediterranean Soils. *Pol J Environ Stud*, **4**, 1479, **2016**.
  39. LI H., RENSSSEN H., ROCHE D.M. Global vegetation distribution driving factors in two Dynamic Global Vegetation Models of contrasting complexities. *Global Planet Change*, **180**, 51, **2019**.
  40. NING T., LI Z., LIU W. Vegetation dynamics and climate seasonality jointly control the interannual catchment water balance in the Loess Plateau under the Budyko framework. *Hydrol Earth Systsc*, **21** (3), 1, **2017**.
  41. ZHANG J., FELZER B.S., TROY T.J., Projected changes of carbon balance in mesic grassland ecosystems in response to warming and elevated CO using CMIP5 GCM results in the Central Great Plains, USA2. *Ecol Model*, **434**, 109247, **2020**.
  42. ZHANG Y.Q., LIU J.B., JIA X., QIN S.G. Soil Organic Carbon Accumulation in Arid and Semiarid Areas after Afforestation: a Meta-Analysis. *Pol J Environ Stud*, **22** (2), 611, **2013**.
  43. POTTER C.S., RANDERSON J.T., FIELD C.B., MASTON P.A., KLOOSTER S.A. Terrestrial ecosystem production: A process model based on global satellite and surface data. *Global Biogeochem Cy*, **7** (4), 811, **1993**.
  44. CAO M.K., WOODWARD F.I. Dynamic responses of terrestrial ecosystem carbon cycling to global climate change. *Nature*, **393** (6682), 249, **1998**.
  45. KANG Z.Q., CHEN J., YUAN D.X., HE S.Y., LI Y.L., CHENG Y., DENG Y., CHEN Y., LIU Y.Y., JIANG G. H., WANG X.Y., ZHANG Q.J. Promotion function of forest vegetation on the water & carbon coupling cycle in karst critical zone: Insights from karst groundwater systems in south China. *J Hydrol*, **590**, 125246, **2020**.
  46. BONAN G.B. Land-atmospheric interactions for climate system models: Coupling biophysical, biogeochemical and ecosystem dynamical processes. *Remote Sens Environ*, **51**, 57-73, **1995**.
  47. LI X.Y., LI Y., CHEN A.P., GAO M.D., SLETTE I.J., PIAO S.L. The impact of the 2009/2010 drought on vegetation growth and terrestrial carbon balance in Southwest China. *Agric For Meteorol*, **269-270**, 239, **2019**.
  48. ZENG X., LI F., SONG X. Development of the IAP Dynamic Global Vegetation Model. *Adv Atmos Sci*, **31** (3), 505, **2014**.
  49. CUI H.R., ZHU X.F., WANG H.G. Collaborative Innovation of Low-Carbon Technology from the Triple Helix Perspective: Exploring Critical Success Factors Based on DEMATEL-ISM. *Pol J Environ Stud*, **29** (2), 1579, **2020**.
  50. DARZI-NAFTCHAI A., KARANDISH F. Adapting rice production to climate change for sustainable blue water consumption: an economic and virtual water analysis. *Theor Appl Climatol*, **135**, 1, **2019**.
  51. MU B., ZHAO X., WU D., WANG X., ZHAO J., WANG H., ZHOU Q., DU X., LIU N. Vegetation cover change and its attribution in China from 2001 to 2018. *Remote Sens*, **13** (3), 496, **2021**.
  52. CHANG X.Q., XING Y.Q., WANG J.Q., YANG H., GONG W.S. Effects of land use and cover change (LUCC) on terrestrial carbon stocks in China between 2000 and 2018. *RCR*, **182**, 106333, **2022**.
  53. MALLAPATY S. How China could be carbon neutral by mid-century. *Nature*, **586** (7830), 482, **2020**.
  54. YAN X.L., BAO Z.X., ZHANG J.Y., WANG G.Q., HE R.M., LIU C.S. Quantifying contributions of climate change and local human activities to runoff decline in the upper reaches of the Luanhe River basin. *J Hydro-environ Res*, **28**, 67, **2020**.
  55. GENG X.J., ZHOU X.C., YIN G.D., HAO F.H., ZHANG X., HAO Z.C., SINGH V.P., FU Y.S.H. Extended growing season reduced river runoff in Luanhe River basin. *J Hydrol*, **582**, 124538, **2020**.
  56. CHEN M., GRIFFIS T.J., BAKER J.M., WOOD J.D., MEYERS T., SUYKER A. Comparing crop growth and carbon budgets simulated across AmeriFlux agricultural sites using the Community Land Model (CLM). *Agric For Meteorol*, **256-257**, 315, **2018**.
  57. WANG M.H., VENEVSKY S., WU C., BERDNIKOV S., SOROKINA V., KULYGIN V. Description of local carbon flux from large scale gridded climate data by a dynamic global vegetation model at variable time steps: Example of Euroflux sites. *Sci Total Environ*, **756**, 143492, **2021**.
  58. SHAO P., ZENG X. Spatiotemporal relationship of leaf area index simulated by CLM3.0-DGVM and climatic factors. *Acta Ecologica Sinica*, **31** (16), 4725, **2011**.
  59. LIANG M.L., XIE Z.H. Anagnostou. Improving the Vegetation Dynamic Simulation in a Land Surface Model

- by Using a Statistical-dynamic Canopy Interception Scheme. *Adv Atmos Sci*, **25** (4), 610, **2008**.
60. COLLATZ G.J., BALL J.T., GRIVET C., BERRY J.A. Physiological and environmental regulation of stomatal conductance, photosynthesis and transpiration: a model that includes a laminar boundary layer. *Agric For Meteorol*, **54**, 107, **1991**.
  61. PAN L., WANG Y.F., SUN Z., QIAO J.J., QIU S.Y., SUN Y.J. Relationship between Leaf Biomass and Radial Growth of *Larix olgensis* Based on Pipe Model Theory. *J Forest Res-Jan*, **2**, 118, **2022**.
  62. LIU S., ZHANG Y.X., LI X., TIAN J.X., WANG W.R. Application of pipe model and the theory of water transportation pattern through tree rings in larch productivity estimation. *Journal of Beijing Forestry University*, **3**, 18, **2021** [In Chinese].
  63. CHIBA Y. Architectural analysis of relationship between biomass and basal area based on pipe model theory. *Ecol Model*, **108**, 219, **1998**.
  64. SWETNAM T.L., FALK D.A. Application of Metabolic Scaling Theory to reduce error in local maxima tree segmentation from aerial LiDAR. *Forest Ecol Manag*, **323** (7), 158, **2014**.
  65. PENG X., YAN W.D., WANG F.Q., ZHAO M.F. Specific leaf area estimation model building based on leaf dry matter content of *Cunninghamia lanceolata*. *Chinese Journal of Plant Ecology*, **42** (2), 209, **2018**.
  66. REICH P.B., WALTERS M.B., ELLSWORTH D.S. From tropics to tundra: Global convergence in plant functioning. *Proceedings of the National Academy of Sciences of the United States of America*, **94** (25), 13730, **1997**.
  67. BONAN G.B., LEVIS S., SITCH S., VERTENSTEIN M., OLESON K.W. A dynamic global vegetation model for use with climate models: concepts and description of simulated vegetation dynamics. *GCB*, **9** (11), 1543, **2003**.
  68. LIU C., LIU B., ZHAO W.Z., ZHU Z.C. Temporal and spatial variability of water use efficiency of vegetation and its response to precipitation and temperature in Heihe River Basin. *Acta Ecologica Sinica*, **40** (3), 888, **2020**.
  69. LIZZI J.M., GARBULSKY M.F. Precipitation controls the annual net primary productivity in sown pastures across a precipitation gradient in dry subtropical Chaco. *J Arid Environ*, **208**, 104863, **2023**.
  70. PAN N., WANG S., WEI F.L., SHEN M.G., FU B.J. Inconsistent changes in NPP and LAI determined from the parabolic LAI versus NPP relationship. *Ecol Indic*, **131**, 108134, **2021**.
  71. LIU J., TANG F., ZHANG G.J., ZHANG P.T. Spatio-temporal distribution of net primary productivity and its driving factors in the Luanhe River Basin from 2000 to 2015. *Chinese Journal of Eco-Agriculture*, **29** (4), 659, **2021**.
  72. YUAN M.S., ZHU Q., ZHANG J., LIU J.X., CHEN H., PENG C.H., LI P., LI M.X., WANG M., ZHAO P.X. Global response of terrestrial gross primary productivity to climate extremes. *Sci Total Environ*, **750**, 142337, **2021**.
  73. LIANG X.L., LIU Z.P., ZHAI L., JI L., FENG Y.J., SANG H.Y. Spatial terrestrial carbon emissions/sequestrations evolution based on ecological network analysis in Beijing-Tianjin-Hebei urban agglomeration. *Ecol Eng*, **189**, 106914, **2023**.
  74. CHI D.K., WANG H., LI X.B., LIU H.H., LI X.H. Assessing the effects of grazing on variations of vegetation NPP in the Xilingol Grassland, China, using a grazing pressure index. *Ecol Indic*, **88**, 372, **2018**.
  75. SUN G.D., MU M. Role of hydrological parameters in the uncertainty in modeled soil organic carbon using a coupled water-carbon cycle model. *Ecol Complex*, **50**, 100986, **2022**.
  76. JEONG S.H., EOM J.Y., LEE J.H., LEE J.S. Effect of rainfall events on soil carbon flux in mountain pastures. *Journal of Ecology and Environment*, **40**, 37, **2017**.
  77. EXBRAYAT J.F., PITMAN A.J., ABRAMOWITZ G., WANG Y.P. Sensitivity of net ecosystem exchange and heterotrophic respiration to parameterization uncertainty. *JGR*, **118** (4), 1640, **2013**.
  78. DILLAWAY D.N., KRUGER E.L. Trends in seedling growth and carbon-use efficiency vary among broadleaf tree species along a latitudinal transect in eastern North America. *Glob Change Biol*, **20**, 908, **2014**.
  79. RIDGEWAY J.R., MORRISSEY E.M., BRZOSTEK E.R. Plant litter traits control microbial decomposition and drive soil carbon stabilization. *Soil Biol Biochem*, **175**, 108857, **2022**.
  80. ZHAO X.C., TIAN P., SUN Z.L., LIU S.G., WANG Q.W., ZENG Z.Q. Rhizosphere effects on soil organic carbon processes in terrestrial ecosystems: A meta-analysis. *Geoderma*, **412**, 115739, **2022**.
  81. CHEN Y.Z., MU S.J., SUN Z.G., GANG C.C., LI J.L., PADARIAN J., GROISMAN P., CHEN J.M., LI S.W. Grassland Carbon Sequestration Ability in China: A New Perspective from Terrestrial Aridity Zones. *Rangeland Ecol Manag*, **69** (1), 84, **2016**.
  82. CONTICELLI, E., PROLI S., TONDELLI S. Integrating energy efficiency and urban densification policies: two Italian case studies. *Energy Build*, **155** (11), 308, **2017**.
  83. CHIMDI A., GURMESSA E. Effects of land use on selected soil properties and carbon sequestration in the Gurra watershed: The case of Chalia District, West Shoa Zone, Oromia, Ethiopia. *S Afr J of Bot*, **156**, 21, **2023**.